crystals

MDPI

Article

Synergistic Antibacterial Activity of Green Synthesized Silver Nanomaterials with Colistin Antibiotic against Multidrug-Resistant Bacterial Pathogens

Mohamed Taha Yassin *, Ashraf Abdel-Fattah Mostafa, Abdulaziz Abdulrahman Al-Askar and Fatimah O. Al-Otibi

Botany and Microbiology Department, College of Science, King Saud University, Riyadh 11451, Saudi Arabia; asali@ksu.edu.sa (A.A.-F.M.); aalaskara@ksu.edu.sa (A.A.A.-A.); falotibi@ksu.edu.sa (F.O.A.-O.)
* Correspondence: myassin2.c@ksu.edu.sa

Abstract: The high frequency of nosocomial bacterial infections caused by multidrug-resistant pathogens contributes to significant morbidity and mortality worldwide. As a result, finding effective antibacterial agents is of critical importance. Hence, the aim of the present study was to greenly synthesize silver nanoparticles (AgNPs) utilizing *Salvia officinalis* aqueous leaf extract. The biogenic AgNPs were characterized utilizing different physicochemical techniques such as energy-dispersive X-ray spectroscopy (EDX), ultraviolet-visible spectrophotometry (UV-Vis), X-ray diffraction analysis (XRD), transmission electron microscopy (TEM), and Fourier transform infrared spectroscopy (FT-IR) analysis. Additionally, the synergistic antimicrobial effectiveness of the biosynthesized AgNPs with colistin antibiotic against multidrug-resistant bacterial strains was evaluated utilizing the standard disk diffusion assay. The bioformulated AgNPs revealed significant physicochemical features, such as a small particle size of 17.615 ± 1.24 nm and net zeta potential value of −16.2 mV. The elemental mapping of AgNPs revealed that silver was the main element, recording a relative mass percent of 83.16%, followed by carbon (9.51%), oxygen (5.80%), silicon (0.87%), and chloride (0.67%). The disc diffusion assay revealed that AgNPs showed antibacterial potency against different tested bacterial pathogens, recording the highest efficiency against the *Escherichia coli* strain with an inhibitory zone diameter of 37.86 ± 0.21 mm at an AgNPs concentration of 100 µg/disk. In addition, the antibacterial activity of AgNPs was significantly higher than that of colistin ($p \leq 0.05$) against the multidrug resistant bacterial strain namely, *Acinetobacter baumannii*. The biosynthesized AgNPs revealed synergistic antibacterial activity with colistin antibiotic, demonstrating the highest synergistic percent against the *A. baumannii* strain (85.57%) followed by *Enterobacter cloacae* (53.63%), *E. coli* (35.76%), *Klebsiella pneumoniae* (35.19%), *Salmonella typhimurium* (33.06%), and *Pseudomonas aeruginosa* (13.75%). In conclusion, the biogenic AgNPs revealed unique physicochemical characteristics and significant antibacterial activities against different multidrug-resistant bacterial pathogens. Consequently, the potent synergistic effect of the AgNPs–colistin combination highlights the potential of utilizing this combination for fabrication of highly effective antibacterial coatings in intensive care units for successful control of the spread of nosocomial bacterial infections.

Keywords: green synthesis; colistin; silver nanoparticles; *Salvia officinalis*; synergism; multidrug resistance

Citation: Yassin, M.T.; Mostafa, A.A.-F.; Al-Askar, A.A.; Al-Otibi, F.O. Synergistic Antibacterial Activity of Green Synthesized Silver Nanomaterials with Colistin Antibiotic against Multidrug-Resistant Bacterial Pathogens. *Crystals* **2022**, *12*, 1057. https://doi.org/10.3390/cryst12081057

Academic Editor: Rocco Caliandro

Received: 10 June 2022
Accepted: 27 July 2022
Published: 29 July 2022

1. Introduction

Antimicrobial resistance (AMR) has evolved as a significant and growing phenomena, resulting in rising healthcare expenses around the world [1]. In recent years, bacterial resistance has been associated with high rates of disease, death, and rising expenses as a result of both prolonged medical care and hospitalization [2]. High incidence of antimicrobial resistance was recently reported in a group of nosocomial bacterial strains known as ESKAPE, which is an abbreviation for *Enterococcus faecium*, *Staphylococcus aureus*,

Klebsiella pneumoniae, *Acinetobacter baumannii*, *Pseudomonas aeruginosa*, *Enterobacter* spp., and *Escherichia coli* pathogens [3].

In this regard, *A. baumannii* is a Gram-negative bacterial strain from the Moraxellaceae family that causes significant nosocomial infections such as ventilator-associated pneumonia (VAP), hospital-acquired pneumonia (HAP), meningitis, urinary tract infections, gastrointestinal infections, bacteremia, and skin/wound infections [4]. Carbapenems were considered the first line of treatment against *A. baumannii*-resistant strains, but their overuse has resulted in an increase in carbapenem resistance in the latest years [5]. Additionally, polymyxins are now extensively utilized as the preferred treatment of multidrug-resistant *A. baumannii* infections while they were primarily avoided because of systemic toxicities such as neurotoxicity and nephrotoxicity [6]. Furthermore, *A. baumannii* is classified as extensive drug resistant (XDR) when it shows resistance to three or more classes of antibiotics (cephalosporins and penicillins, aminoglycosides, fluoroquinolones, and carbapenems), whereas pandrug-resistant (PDR) *A. baumannii* is an XDR isolate resistant to tigecycline and polymyxins [7]. The multidrug-resistant *A. baumannii* HAP and VAP infections resulted in a high mortality rate, culminating in a 56.2% total mortality rate [8].

The other Gram-negative bacterial stain, *K. pneumoniae* of the Enterobacteriaceae family, poses a significant concern because it is normally found in the gastrointestinal tract microbiome of humans [9]. This bacterium is an opportunistic pathogen that causes cystitis, urinary tract infections, life-threatening infections such endocarditis and septicemia, pneumoniae, and surgical wound infections [10]. Alarmingly, *K. pneumoniae* nosocomial bacterial strains accounted for roughly one-third of all Gram-negative infections, resulting in a high death rate, longer hospitalizations, and expenses [11]. After *Clostridium difficile* and *Staphylococcus aureus*, *Klebsiella* species have been recognized as the third main cause of HAIs in the United States (9.9%) [12]. *Klebsiella pneumoniae* strains have been identified as the second most common cause of bloodstream infections, with a death rate of up to 50% [13].

The other member of the Enterobacteriaceae family, namely *Enterobacter*, is a rod-shaped Gram-negative, facultatively anaerobic bacteria, non-spore-forming, lactose-fermenting, and urease-positive bacterial strain [14]. Antimicrobial resistance of *Enterobacter* spp. could be due to the production of beta-lactamases, which have the ability to hydrolyze the beta-lactam ring in cephalosporins and penicillin [15]. The clinical isolates of *Enterobacter* spp. in intensive care units (ICUs) were considered as the third most common pathogen in respiratory tract infections, the fourth among surgical wound infections, and the fifth among nosocomial urinary tract and bloodstream infections [16]. In the United States, *Enterobacter* spp. were reported to be the second main carbapenem-resistant Enterobacteriaceae, contributing to the high incidence of carbapenem-resistant infections [17]. *Enterobacter cloacae* complex (ECC) were reported as nosocomial bacterial pathogens causing a range of infections such as urinary tract infections, pneumonia, and septicemia [18].

Another ESKAPE pathogen is *Escherichia coli*, particularly uropathogenic *E. coli* strains (UPEC), which are responsible for roughly 50% of hospital-acquired infections, 95% of community-acquired infections, and are the most common pathogen in complex urinary tract infections [19]. Excessive use of antibiotics for treatment of urinary tract infections has resulted in a high incidence of multidrug-resistant bacterial strains [20]. In this regard, a previous study in Egypt investigated the resistance patterns of *E. coli* strains isolated from outpatients with community-acquired urinary tract infections and found that 62% of the total *E. coli* isolates had multidrug resistance profiles [21]. On the other hand, *P. aeruginosa* is another Gram-negative pathogen that is linked to a wide range of hospital-acquired infections, including bloodstream infections and ventilator-associated pneumonia [22]. This bacterium was reported to be the fourth etiological agent of nosocomial infections, responsible for about 10% of hospital-acquired infections [23]. It is also the second most common causative agent of pneumonia and the third most common Gram-negative etiological agent of bloodstream infections [24].

Apart from ESKAPE pathogens, *Salmonella* was described as the most frequent etiological agent of food poisoning infections, causing an estimated 1 million illnesses, 20,000 hospitalizations, and 400 fatalities each year in the United States, resulting in economic losses of $3.3 to 4.4 billion [25,26]. *Salmonella typhimurium* infections have shown a persistent lack of sensitivity to conventional antibiotics, possibly as a result of *Salmonella*'s vast host range, which could lead to antibiotic resistance spreading to other bacterial strains [27]. The mechanisms of antibacterial resistance can be divided into three categories: the first is through reduced membrane permeability, which increases drug efflux; the second is through genetic mutations or post-translational modifications; and the third is through direct inactivation of the drug through hydrolysis or modification [28]. Taken together, antibacterial resistance is a global burden that necessitates the development of novel antimicrobial agents to combat the rise of multidrug-resistant strains in hospitals and intensive care units.

Nanomaterials are regarded as a possible platform to counteract the increased incidence of antibacterial resistance due to their physicochemical features, recording nanoscale dimensions of 1–100 nm [29]. Nanoparticles have special features in this regard, such as improved solubility and stability, simplicity of synthesis, and biocompatibility [30]. The high surface to volume ratio and ultra-small size of these nanoparticles were their most distinguishing characteristics [31]. Moreover, nanomaterials comprise nanoparticles containing Ce, Ag, Cu, Au, Al, Mg, Pd, Zn, Ti, Se, Cd, Ni, and super-paramagnetic Fe whereas silver nanoparticles (AgNPs) were found to possess the highest antimicrobial efficiency compared to other metallic nanoparticles such as CuONPs, TiONPs, AuNPs, and Fe_3O_2NPs [32,33]. Silver nanoparticles could be formulated using a chemical reduction or a green approach using microbial or plant extracts [34]. The chemical approach to AgNPs synthesis resulted in the adsorption of hazardous toxic chemicals on the nanoparticles' surface, increasing their toxicity, whereas the green method used safe reducing agents for the formulation of silver nanoparticles [35]. Additionally, the chemical technique of AgNPs synthesis is expensive and necessitates extra steps to prevent particles from aggregating [36]. In contrast, safer stabilizing and reducing agents have been utilized for green formulation of AgNPs nanoparticles, particularly the use of plant extracts [37]. Furthermore, the reaction process for AgNPs synthesis utilizing plant extracts takes place under natural conditions without being restricted by harsh or rigorous reaction conditions. Plant extract-based nanoparticles are considered as a safe, affordable, and eco-friendly alternative for antibacterial applications [38].

The biogenic silver nanomaterials mediated cell death via a number of mechanisms, including cell wall disruption, disturbance of cell membrane permeability, production of reactive oxygen species (ROS), and inactivation of respiratory enzymes [39].

Salvia officinalis L. (Sage) belongs to the Lamiaceae family and was reported to possess anti-inflammatory, anticarcinogenic, antioxidant, hypolipidemic, and hypoglycemic properties [40]. The biogenic AgNPs formulated using *S. officinalis* leaf extract exhibited antimicrobial efficacy against Gram-negative strains such as *P. aeruginosa*, *K. pneumoniae*, and *Proteus mirabilis* strains, recording suppressive zone diameters ranging from 20.7–23.0 mm [41]. Another report demonstrated the antibacterial efficiency of AgNPs formulated using *S. officinalis* aqueous leaf extract against three Gram-positive bacterial strains namely, *S. aureus*, *B. subtilis*, and MRSA (methicillin-resistant *Staphylococcus aureus)* [42].

Colistin, a polymyxin E compound, was initially used in a clinical setting in 1959 and is now considered a last-line treatment option for multidrug-resistant Gram-negative bacterial infections [43]. Recently, several reports indicated the incidence of colistin resistance among nosocomial ESKAPE pathogens such as *K. pneumonia* [44], *A. baumannii* [45], *P. aeruginosa* [46], *E. coli* [47], and *E. cloacae* [48]. A previous study reported the synergistic antibacterial effectiveness of AgNPs combined with colistin on decellularized human amniotic membrane against *P. aeruginosa* and *K. pneumoniae* strains [49]. Collectively, the previous reports investigated the antimicrobial efficiency of AgNPs synthesized using *S. officinalis* extract without investigating the synergistic efficiency of these nanomateri-

als with colistin antibiotic against the nosocomial bacterial pathogens with a significant resistance pattern.

Because of the reported colistin resistance of ESKAPE pathogens, new antimicrobial combinations are needed to combat the high prevalence of the multidrug-resistant bacterial strains in hospital settings and intensive care units. Hence, the aim of the present study was to evaluate the antimicrobial effectiveness of green synthesized AgNPs utilizing aqueous leaf extract of *S. officinalis* against five bacterial strains causing nosocomial infections, namely, *K. pneumonia*, *E. coli*, *P. aeruginosa*, *A. baumannii*, and *E. cloacae*, and against the food poisoning bacterial strain *S. typhimurium*. Moreover, the synergistic antimicrobial efficacy of the biogenic silver nanomaterials with colistin antibiotic was examined.

2. Materials and Methods

2.1. Salvia officinalis Water Extract Preparation

Leaves of *S. officinalis* were procured from a local market in Riyadh, Saudi Arabia. The herbarium of the Botany and Microbiology Department, College of Science, King Saud University, recognized the collected plant materials. The leaves of *S. officinalis* were rinsed three times with distilled water after being washed with tap water. *S. officinalis* leaves were homogenized using a mechanical mortar to achieve a fine powder. Then, 50 g powder was immersed in 500 mL flasks containing 200 mL distilled H_2O, and the flask was heated at 50 °C for 30 min. Finally, the extract was agitated at 25 °C for 24 h using a magnetic stirrer. To obtain clear filtrate, filtration of the *S. officinalis* extract was achieved using Whatman filter paper (1), and finally refrigerated at 4 °C for subsequent use [50–53].

2.2. Green Formulation of AgNPs

Green formulation of silver nanomaterials was accomplished by the addition of 10 mL aqueous leaf extract of *S. officinalis* to 90 mL 1 mM solution of silver nitrate ($AgNO_3$). Silver nitrate ($AgNO_3$) salt was acquired from Sigma-Aldrich, Missouri, USA. Incubation of the reaction mixture was achieved under dark conditions at 24 °C in a shaking incubator. The shift in color of the silver nitrate solution from colorless to dark brown indicated AgNPs formation. The biosynthesized silver nanomaterials were gathered by centrifugation of the bioreduced mixture at 10,000 rpm for 10 min. Finally, the biosynthesized AgNPs were washed thrice with distilled water to remove any impurities and then dried in oven at 80 °C. The obtained AgNPs were subjected to subsequent examination and investigation.

2.3. Characterization of the Biosynthesized AgNPs

The physicochemical features of the biogenic AgNPs were investigated using various techniques. In this regard, UV-Vis spectral analysis of the biosynthesized silver nanomaterials formulated utilizing *S. officinalis* extract was performed using a UV-Vis spectrophotometer (UV-1601, Shimadzu, Japan). Prior to analysis, the biogenic AgNPs were sonicated, and a drop of the diluted sample was dropped onto a carbon-coated copper grid. After, the biogenic AgNPs' size and shape were investigated using a transmission electron microscope (JEOL, JEM1011, Tokyo, Japan) (JEOL, JEM1011, Tokyo, Japan). The functional groups of the biogenic AgNPs were investigated using Fourier transform infrared (FTIR) spectral analysis to determine these groups contributing to biosynthesized AgNPs' reduction and stabilization. On the other hand, the elemental composition of the biosynthesized silver nanomaterials was detected utilizing a scanning electron microscope (SEM) fitted with an energy-dispersive X-ray (EDX) analyzer (JEOL, JSM-6380 LA, Tokyo, Japan). The crystalline features of the biosynthesized AgNPs were characterized using a Shimadzu XRD model 6000 diffractometer (Japan) fitted with a graphite monochromator. Finally, the zeta potential analysis and dynamic light scattering (DLS) of the biosynthesized AgNPs were investigated utilizing a Zeta sizer instrument (Malvern Instruments Ltd.; zs90, Worcestershire, UK) to detect the AgNPs' surface charge and average hydrodynamic diameter of the biosynthesized AgNPs [54,55]. Inductively coupled plasma mass spectrometry (ICP-MS)

measurements were carried out to detect the concentration of the biosynthesized silver nanoparticles [56].

2.4. Screening of the Antibacterial Effectiveness of the Biosynthesized AgNPs

Six bacterial strains namely, namely, *A. baumannii* (ATCC 43498), *K. pneumoniae* (ATCC 700603), *E. coli* (ATCC 25922), *Enterobacter cloacae* (ATCC 13047), *P. aeruginosa* (ATCC 9027), and *S. typhimurium* (ATCC 14023), were attained from the American Type Culture Collection. The chosen strains were selected for the bacteriostatic studies because they have recently significantly contributed to global mortality and morbidity due to their high levels of antibiotic resistance. The disk diffusion method was utilized to investigate the antimicrobial efficiency of the green synthesized AgNPs against the detected bacterial strains [57]. The bacterial colonies were harvested using a sterile loop, dispersed in the saline solution, and the turbidity of the bacterial suspension was accustomed utilizing the 0.5 McFarland standard to obtain a viable cell count of 10^8 cfu/mL. Sterile Mueller Hinton agar (MHA) medium was poured in sterile Petri dishes and then the poured plates were inoculated with 0.5 mL bacterial suspension. The biogenic silver nanomaterials were dissolved in methanol solvent and then sonicated for complete solubility. Then, sterile filter paper disks (8 mm in diameter) were impregnated with 50 and 100 µg of the dissolved AgNPs. After, the loaded disks were placed over the previously prepared MHA plates seeded with the bacterial suspension. Colistin sulfate (CAS No.1 264-72-8, purity $\geq$ 99.9%) was purchased from Sigma-Aldrich (St. Louis, MO, USA). Filter paper disks impregnated only with methanol solvent served as negative controls, whereas filter paper disks loaded with 10 µg colistin served as positive controls. The bacterial strain was considered colistin resistant if the inhibition zone diameter was $\leq$10 while the strain was considered sensitive if the inhibition zone diameter $\geq$ 11 mm. The plates were refrigerated for 2 h in the refrigerator to permit diffusion of silver nanoparticles, then incubated at 37 °C for 24 h, and, finally, the inhibition zone diameters were detected using a Vernier caliper. The broth microdilution assay was carried out to detect the minimum inhibitory concentration (MIC) of the *S. officinalis* AgNPs against the *E. coli* strain with the highest susceptibility to the biosynthesized AgNPs using 96-well microtiter plates, as demonstrated in a previous report [58]. Moreover, the minimum bactericidal concentration (MBC) was investigated by streaking inoculums from MIC wells onto freshly prepared MHA plates. Then, the plates were incubated at 37 °C for 24 h and finally the plates were checked for microbial growth. MBC was the lowest concentration of silver nanomaterials that demonstrated no bacterial growth [59,60].

2.5. Determination of Synergistic Efficiency of the Bioformulated AgNPs with Colistin Antibiotic

The synergistic activity of the biosynthesized silver nanomaterials combined with colistin antibiotic against the concerned bacterial strains was detected using the standard disk diffusion method [61,62]. The sterilized filter paper disks (8 mm in diameter) were loaded with 10 µg/disk of colistin antibiotic while another group of disks were loaded with the MIC concentration of the biosynthesized silver nanoparticles (10 µg/disk), and a third group of disks were loaded with both colistin antibiotic (10 µg/disk) and the minimal inhibitory concentration of AgNPs (10 µg/disk) for the detection of the synergistic activity of the biogenic silver nanomaterials. Additionally, filter paper disks loaded with methanol solvent only served as negative controls. As previously stated, the seeded MHA plates were prepared, and then the impregnated disks were put over the seeded plates. Finally, the plates were refrigerated for 2 h to permit AgNPs diffusion and then the plates were incubated at 25 °C for 24 h. The suppressive zone diameters were detected using a Vernier caliper and the synergistic effectiveness of the biosynthesized AgNPs was detected according to the following equation: Synergism % = $\frac{B-A}{A} \times 100$, where A is the inhibition zone diameter of colistin antibiotic and B is the suppressive zone diameter of colistin antibiotic + AgNPs [63].

2.6. Statistical Analysis

The antibacterial and synergistic activity data of AgNPs were statistically analyzed utilizing GraphPad Prism 5.0 (GraphPad Software, Inc., La Jolla, CA, USA) with one-way analysis of variance and Tukey's test. The data was presented as the mean of triplicates ± standard error.

3. Results and Discussion

3.1. Green Synthesis of Silver Nanomaterials

The biosynthesis of AgNPs was demonstrated by the change in the color of the silver nitrate solution ($AgNO_3$) from colorless to dark brown after the addition of *S. officinalis* aqueous extract, as shown in Figure 1. In this regard, the observed color change could be assigned to the reduction of Ag^+ ions to the metallic nano-silver (Ag°) through the action of the active metabolites involved in *S. officinalis* extract as shown in Figure 2 [64]. The UV-Vis spectrum of the biogenic AgNPs demonstrated the presence of three absorption peaks at 242, 334, and 395 nm (Figure 3). The surface plasmon resonance (SPR) of the biogenic AgNPs was shown by the peak at 395 nm, which was consistent with a previous study that disclosed the green synthesis of AgNPs utilizing Jalapeo Chili extract, displaying surface plasmon resonance centered at 395 nm. [65]. Another study confirmed the same findings, showing that biogenic AgNPs synthesized with *Chara* algae extract exhibited surface plasmon resonance at 395 nm [66].

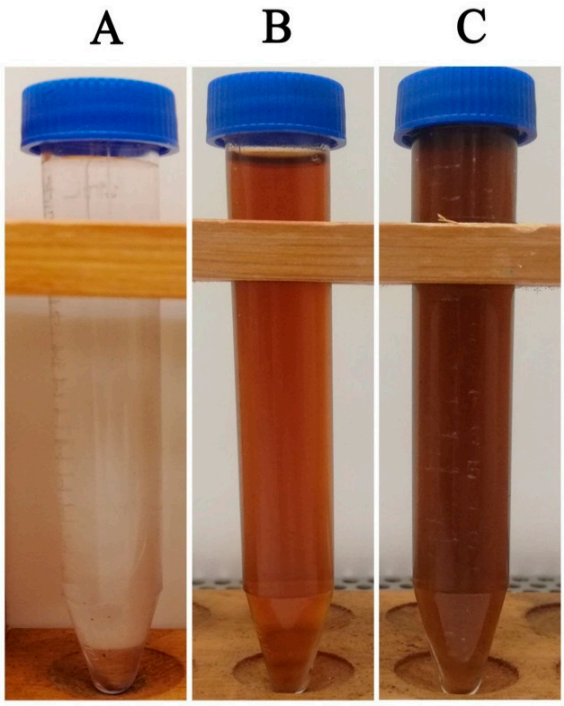

Figure 1. Change in the color of $AgNO_3$ solution after the addition of *S. officinalis* extract. (**A**): colorless $AgNO_3$ solution; (**B**): water extract of *Salvia officinalis* leaves; (**C**): AgNPs dark brown solution.

The AgNPs synthesis in the previous study was performed utilizing ethanolic extract of *S. officinalis* leaves while in our current study, the biosynthesis of AgNPs was achieved using aqueous extract of *S. officinalis* leaf extract [41]. The synthesis method in our study is an ecofriendly and cost-effective method compared to the previous report.

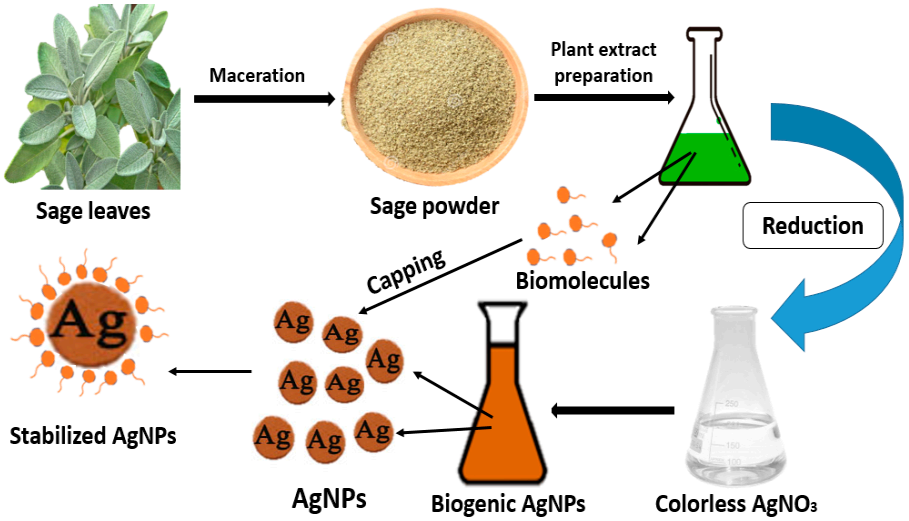

Figure 2. Schematic illustration of the preparation of the biogenic AgNPs utilizing *S. officinalis* aqueous leaf extract.

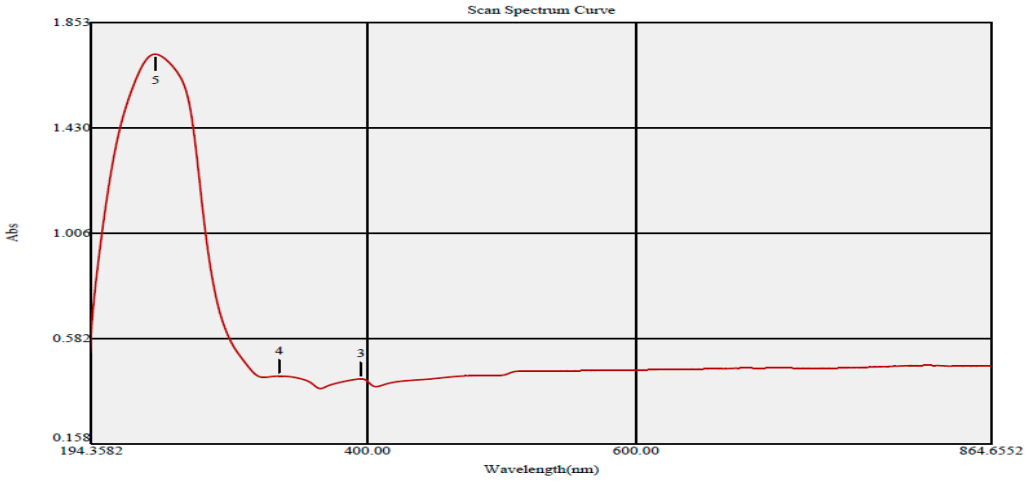

Figure 3. UV-vis spectrum of the biogenic AgNPs formulated using *S. officinalis* extract (peak 3: 395 nm; peak 4: 334 nm; peak 5: 242).

3.2. TEM Analysis of the Biogenic AgNPs

Transmission electron microscopy (TEM) examination was found to be the most effective method for detecting AgNPs' size and shape [67]. The TEM micrographs revealed the formation of well-dispersed spherical nanoparticles with an average size diameter ranging from 5–60 nm as shown in Figure 4. The particle size distribution histogram was plotted to detect the average particle size diameter of the biosynthesized AgNPs. In this setting, the estimated average diameter of the synthesized AgNPs was 17.615 ± 1.24 nm (Figure 5). The small diameter of the synthesized silver nanomaterials revealed the high effectiveness in utilizing the green approach for AgNPs synthesis [68].

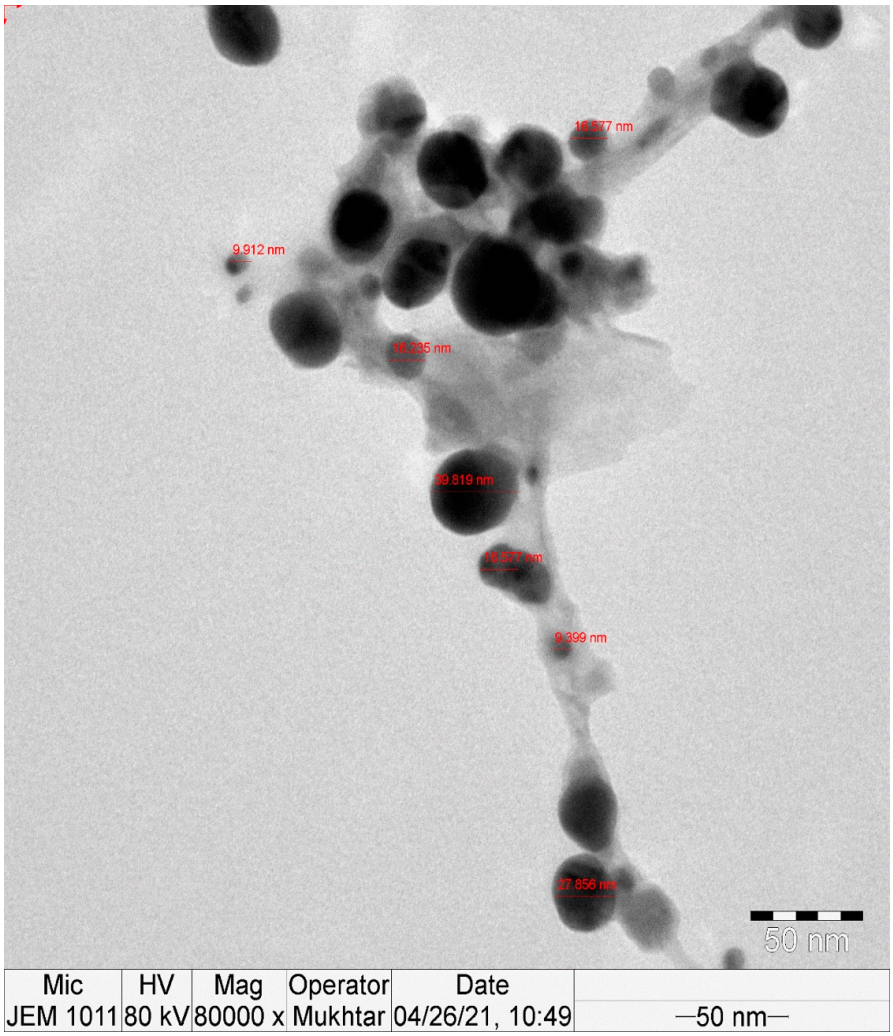

Figure 4. TEM micrographs of the biosynthesized AgNPs.

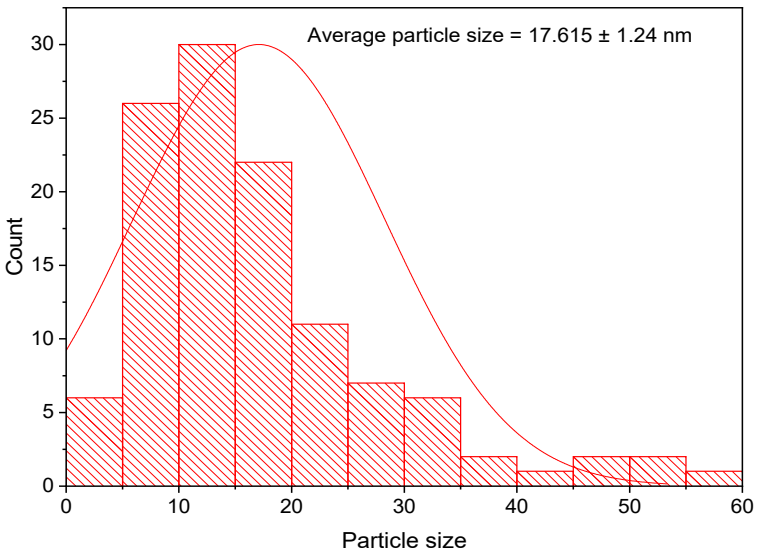

Figure 5. Particle size distribution histogram of the biosynthesized silver nanomaterials (number of analyzed particles = 116).

3.3. EDX Investigation of the Biogenic AgNPs

The elemental mapping of the biosynthesized AgNPs was detected using energy-dispersive X-ray (EDX) analysis. The analysis indicated that the biogenic AgNPs were composed of the following elements: carbon (9.51%), oxygen (5.80%), silicon (0.87%), chloride (0.67%), and silver (83.16%), as shown in Figure 6. The traces of carbon could be assigned to the carbon tape used during sample processing while the minor peak of oxygen could be attributed to the emission of X-rays from free amino groups [69]. Furthermore, the weak peaks of silicon and chloride may be due to X-ray emissions from sugars or proteins present in the extract [70]. On the other hand, a strong peak of silver was detected at 2.983 keV, recording a relative mass percentage of 83.16%. The high percentage of silver revealed the high efficiency of the green synthesis approach of silver nanoparticles synthesis utilizing *S. officinalis* leaf extract.

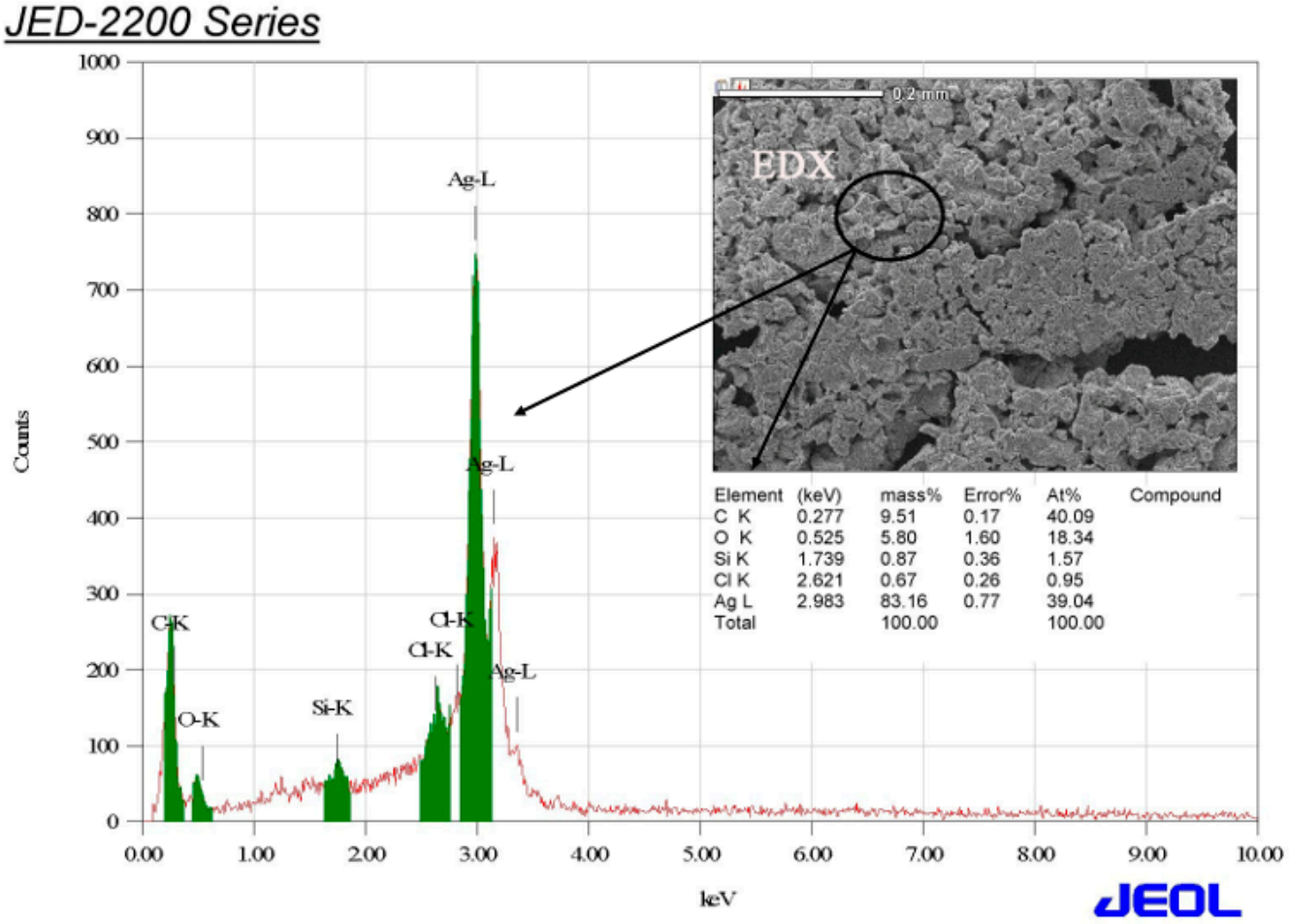

Figure 6. EDX analysis and SEM micrograph of the biosynthesized silver nanomaterials formulated using *S. officinalis* extract.

3.4. Fourier Transform Infrared Spectroscopy (FT-IR) Analysis of the Biosynthesized Silver Nanomaterials

Different functional groups responsible for the reduction and stabilization of biosynthesized AgNPs were identified using the FTIR technique [71]. The FTIR spectrum revealed the presence of four absorption peaks at 3433.23, 1627.87, 1261.82, and 570.17 cm^{-1} (Figure 7). The broad absorption peak at 3433.23 cm^{-1} was allocated to the O-H stretching of phenolic compounds of *S. officinalis* extract. In this regard, the biosynthesized AgNPs were stabilized by the polyphenolic compounds of *S. officinalis* extract [72]. A previous study demonstrated that the phenolic functional groups of *R. officinalis* leaf extract mediated a reduction of $AgNO_3$ and stabilization of the biogenic AgNPs [73]. In addition, the absorption band at

1627.87 cm^{-1} indicated the C=C stretching of conjugated alkenes while the weak absorption band at 1261.82 cm^{-1} revealed C-N stretching of aromatic amines. The weak band detected at 801.29 cm^{-1} revealed the C=C bending of alkenes. Furthermore, the absorption band at 570.17 cm^{-1} was assigned to the functional group of metal oxygen bonds, indicating the molecular motion of Ag-O stretching as shown in Table 1 [74,75].

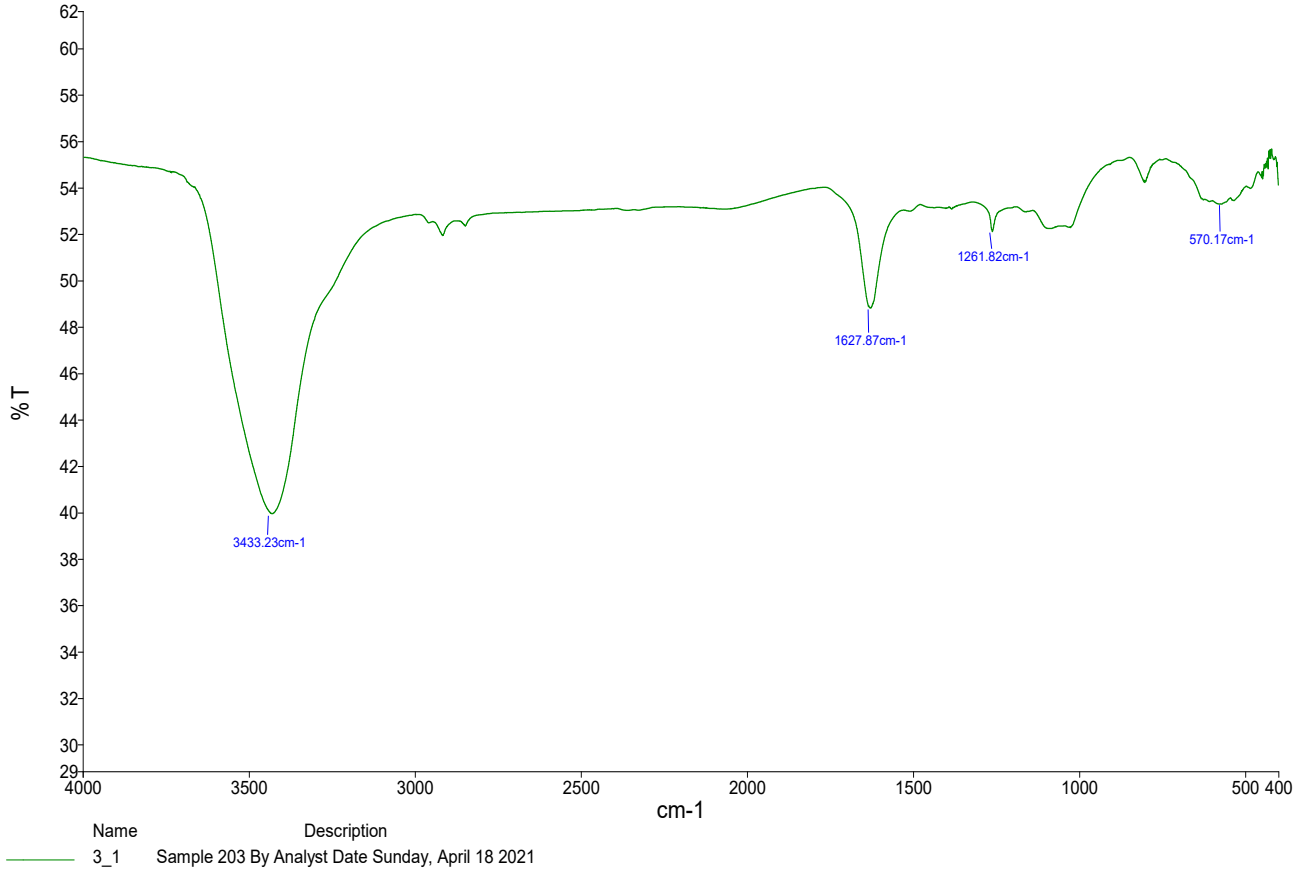

Figure 7. FTIR spectrum of silver nanoparticles formulated using *S. officinalis* extract.

Table 1. Functional groups of the biogenic AgNPs detected using FTIR analysis.

No.	Absorption Peak (cm^{-1})	Appearance	Functional Groups	Molecular Motion
1	3433.23	Strong, broad	Alcohols and phenols	O-H stretching
2	1627.87	Medium	Conjugated alkene	C=C stretching
3	1261.82	Weak	Aromatic amines	C-N stretching
4	801.29	Weak	Alkenes	C=C bending
5	570.17	Weak, broad	metal oxygen bond (AgNPs)	Ag-O stretching

3.5. XRD Analysis of the Biosynthesized Silver Nanomaterials

XRD analysis demonstrated the presence of three diffraction peaks at 2θ degrees of 38.148, 44.291, and 64.609°, corresponding to the planes of silver crystals (111), (200), and (220), respectively, as demonstrated in Figure 8. These results indicated the biosynthesis of face-centered cubic (*fcc*), confirming the crystalline nature of the biofabricated AgNPs. Our findings are consistent with a previous report that indicated the mycosynthesis of green AgNPs using *Aspergillus brunneoviolaceus*, with an XRD spectrum showing diffraction peaks at 2θ degrees of 37.96°, 46.08°, 64.4°, 76.83°, and 81.1° corresponding to the planes (111), (200), (220), (311), and (222), indicating the crystallographic nature of the face-centered cubic (*fcc*) Ag [76]. Another report confirmed the green synthesis of biogenic AgNPs using

Rhizopus stolonifer with an XRD pattern showing three diffraction peaks at 2θ degrees of 37.65°, 44.85°, and 64.89°, corresponding to the planes (111), (200), and (220), respectively, which affirmed the crystallographic nature of the biosynthesized AgNPs [77].

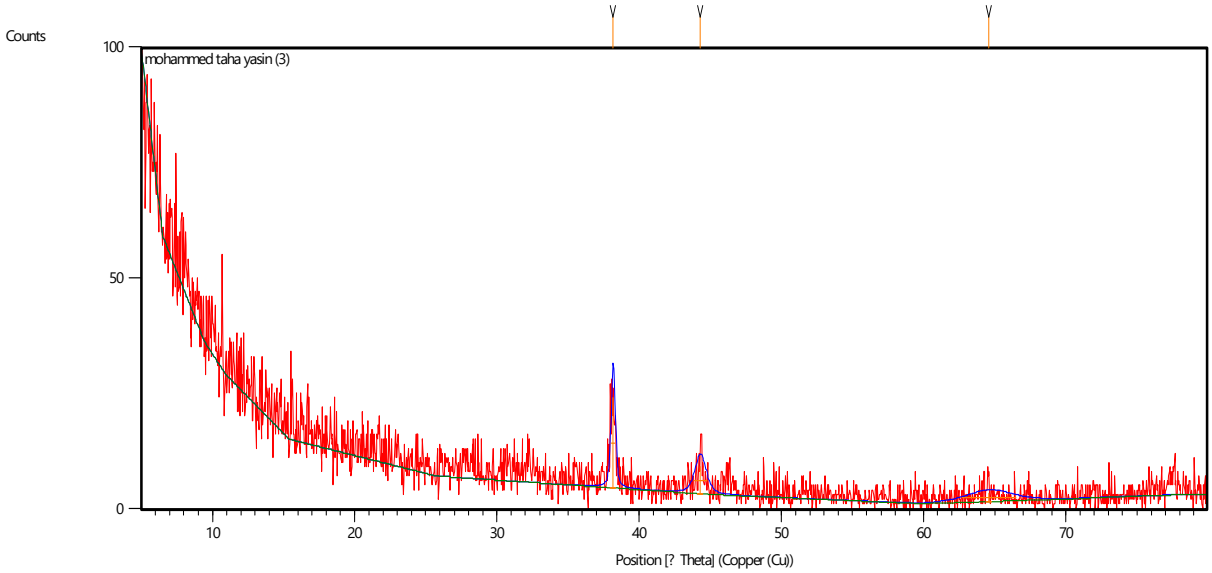

Figure 8. XRD pattern of the biosynthesized silver nanomaterials.

3.6. Zeta Potential and ICP-MS Measurements of the Biogenic AgNPs

The hydrodynamic size of AgNPs was investigated using the dynamic light scattering (DLS) method while the surface charge of the nanomaterials was investigated using the zeta potential analysis technique [78]. The biogenic AgNPs revealed an average hydrodynamic size of 44 nm with a polydispersity index of 0.582, as demonstrated in Figure 9. The particle size of the silver nanoparticles detected by DLS was larger than that estimated by TEM examination, which could be due to the accumulation of extra hydrate layers on the surface of the silver nanomaterials [79].

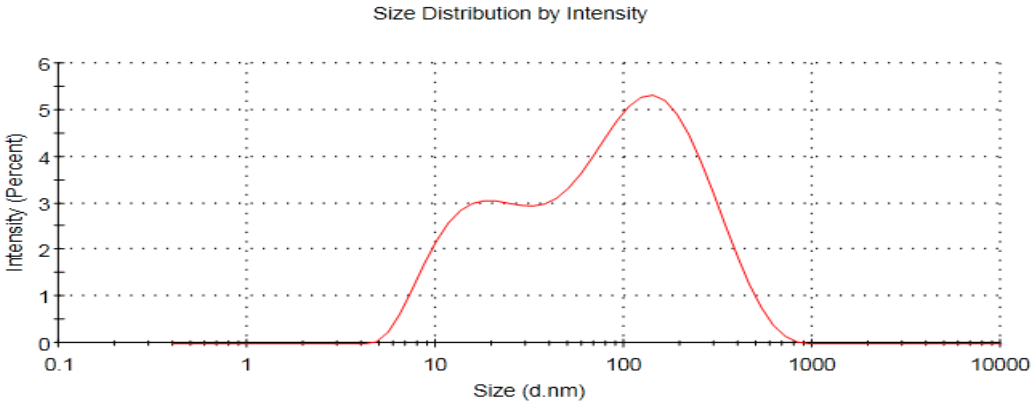

Figure 9. Dynamic light scattering pattern of the biosynthesized silver nanoparticles.

The surface charge of the biosynthesized silver nanomaterials was investigated using zeta potential analysis. The estimated zeta potential value of AgNPs was −16.2 mV (Figure 10). The biomolecules of *S. officinalis* capped on the surface of the biosynthesized AgNPs may be accountable for the negative charge on their surface [80]. Accordingly, the negative charge of AgNPs contributed to the electrostatic repulsion between them, contributing to their stability in aqueous solutions [81]. The estimated concentration of the biogenic AgNPs was 72 × 10^9 particles/mL, corresponding to total mass concentration of 10 mg/mL.

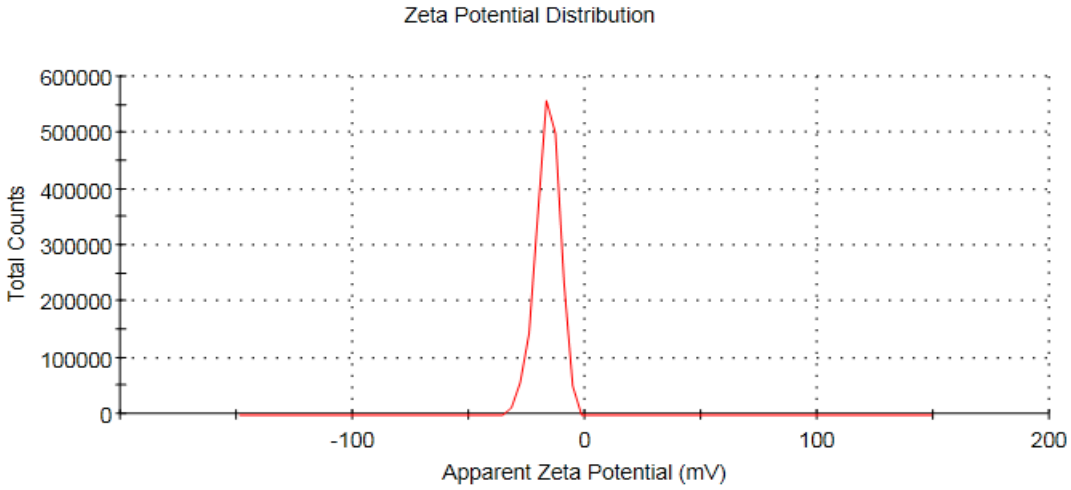

Figure 10. Zeta potential analysis of the biogenic silver nanomaterials.

3.7. Screening of Antibacterial Effectiveness of AgNPs against the Pathogenic Bacterial Strains

The biosynthesized AgNPs were screened for their antimicrobial efficacy against the tested bacterial pathogens using the standard disk diffusion method. The *E. coli* strain displayed the maximum susceptibility to the biosynthesized AgNPs at both 50 and 100 µg/disk, recording suppressive zones of 31.24 ± 0.18 and 37.86 ± 0.21 mm, respectively (Table 2). In contrast, the *P. aeruginosa* strain showed the least sensitivity, recording suppressive zones of 14.27 ± 0.08 and 17.43 ± 0.45 mm to both AgNPs concentrations of 50 and 100 µg/disk, respectively. Our results are consistent with that of Balčiūnaitienė et al., 2020, who reported the antimicrobial efficiency of AgNPs synthesized using *S. officinalis* leaf extract, recording an inhibitory zone range of 20.7–23.0 mm against *P. aeruginosa*, *K. pneumoniae*, and *P. mirabilis* strains [41]. Interestingly, the biogenic AgNPs exhibited antibacterial activity against the colistin-resistant *A. baumannii*, strain which was significantly higher than that of colistin antibiotic. In this setting, the bacterial strain developed resistance to the antibiotic colistin through chromosomal gene mutations that resulted in structural change in the lipid A component of lipopolysaccharide, which is the main target of colistin [82]. The structural modifications of the lipid A component include the addition of 4-amino-4-deoxy-L-arabinose (L-Ara4N) and phosphoethanolamine (PEtN) to the phosphate groups of lipid A [83]. The biosynthesized AgNPs, on the other hand, were presumed to exhibit antibacterial efficacy against the bacterial pathogens through a variety of mechanisms. Continuous silver ion discharge from silver nanoparticles may act as a microbe-killing method [84]. The estimated concentration of Ag ions was 72 billion per ml as estimated by ICP-MS analysis.

Table 2. Antimicrobial effectiveness of the biogenic AgNPs against the tested bacterial strains.

The Tested Strains	Inhibition Zone Diameter (mm)			
	AgNPs (50 µg/Disk)	AgNPs (100 µg/Disk)	Colistin (10 µg/Disk)	Negative Control
A. baumannii	16.91 ± 0.11	19.47 ± 0.29	9.97 ± 0.34	0.00 ± 0.00
E. coli	31.24 ± 0.18	37.86 ± 0.21	26.41 ± 0.51	0.00 ± 0.00
E. cloacae	19.16 ± 0.13	22.09 ± 0.32	13.48 ± 0.16	0.00 ± 0.00
K. pneumoniae	25.18 ± 0.27	28.45 ± 0.41	19.43 ± 0.36	0.00 ± 0.00
P. aeruginosa	14.27 ± 0.08	17.43 ± 0.45	15.41 ± 0.38	0.00 ± 0.00
S. typhimurium	21.63 ± 0.34	24.37 ± 0.11	16.12 ± 0.24	0.00 ± 0.00

To begin with, silver ions have a proclivity for binding to phosphorous- and sulfur-containing compounds, which are known to be important components of DNA, proteins, and cell membranes [85]. In addition, silver ions can disrupt sulfur-containing enzymes,

which are abundantly located in cell membrane [86]. Silver ions bind to thiol (–SH) functional groups of sulfur-containing enzymes, forming S–Ag linkages, which inactivate ion transport and transmembrane energy-generating enzymes in the cell membrane [87]. Moreover, the production of reactive oxygen species (ROS) by silver nanomaterials contributes to the disruption of cellular constituents of bacterial cells [88]. For example, ROS produced by silver ions interrupt the hydrogen bonds between the two antiparallel polynucleotide strands of DNA molecules, resulting in denaturation of DNA through intercalation between pyrimidine and purine base pairs [89]. The minimum inhibitory concentration of the biosynthesized silver nanomaterials was evaluated against the *E. coli* strain, which exhibited the highest susceptibility to AgNPs. The minimal inhibitory concentration of the biogenic AgNPs against the *E. coli* strain was found to be 10 µg/mL whereas the minimal bactericidal concentration was found to be 15 µg/mL. The antibacterial effectiveness of biosynthesized silver nanoparticles at low concentrations could be credited to the small particle size of 17.615 ± 1.24 nm, which would allow the silver nanoparticles to penetrate easily into bacterial cell membranes, allowing them to attack various bacterial cellular targets [90].

3.8. Synergistic Antibiotic Activity with Colistin Antibiotic against the Tested Bacterial Pathogens

Our study investigated the synergistic antibacterial activity of green synthesized AgNPs utilizing aqueous leaf extract of *S. officinalis* with colistin antibiotic against the *K. pneumonia*, *E. coli*, *P. aeruginosa*, *A. baumannii*, *E. cloacae*, and *S. typhimurium* strains as the previous reports indicated that these strains exhibited high antimicrobial resistance to different classes of antibiotics [7,9,17,21,27].

The synergistic antibacterial effectiveness of the MIC concentration of AgNPs with colistin antibiotic was investigated against the concerned bacterial pathogens using the standard disk diffusion method (Figure 11). Interestingly, the biogenic silver nanoparticles exhibited the highest synergistic efficiency with colistin antibiotic against the multidrug-resistant *A. baumannii* strain, recording a synergistic proportion of 85.57% (Figure 12). The combined action of colistin and AgNPs exhibited antibacterial efficiency against the *A. baumannii* strain, recording an inhibitory zone diameter of 18.78 ± 0.16 mm, which was significantly higher than that of colistin antibiotic only (Table 3). Moreover, the biogenic AgNPs revealed synergistic effectiveness with the colistin antibacterial agent against *E. cloacae*, *E. coli*, *K. pneumoniae*, and *S. typhimurium*, recording relative synergism percentages of 53.63, 35.76, 35.19, and 33.06%, respectively. On the other hand, weak synergistic activities of the biosynthesized AgNPs with colistin antibiotic against the *P. aeruginosa* strain were observed, recording a relative synergism percentage of 13.75%. A previous study indicated that silver nanomaterials revealed synergistic activity with amikacin antibiotic against *A. baumannii* and *E. coli* whereas ampicillin antibiotic revealed synergism with AgNPs against the *A. baumannii* strain only [91]. In addition, another study demonstrated that the chemically synthesized AgNPs revealed synergistic efficiency with kanamycin, enoxacin, tetracycline, and neomycin antibiotics against *Salmonella* strains [92]. This study also demonstrated the mode of synergism, proposing a four-step mechanism that begins with the formation of complexes between tetracycline and AgNPs, which then attach to the bacterial surface, causing toxicity to bacterial cells by binding to DNA and protein molecules, disrupting cell function, and finally leading to the initiation of cell death. Another study reported synergistic antibacterial activity between ampicillin and AgNPs at lower concentrations of 0.03 and 2.5 mg/L, respectively, whereas no synergistic activity was detected between chemically synthesized AgNPs and each of ciprofloxacin, oxacillin, ceftazidime, and meropenem antibiotics against *E. coli* CCM 4225, *S. aureus* CCM 4223, and *P. aeruginosa* CCM 3955 strains [93]. Accordingly, the synergistic bioactivity of the biosynthesized AgNPs with colistin antibiotic indicated that the AgNPs–colistin combination could be a promising antibacterial agent against multidrug-resistant pathogens.

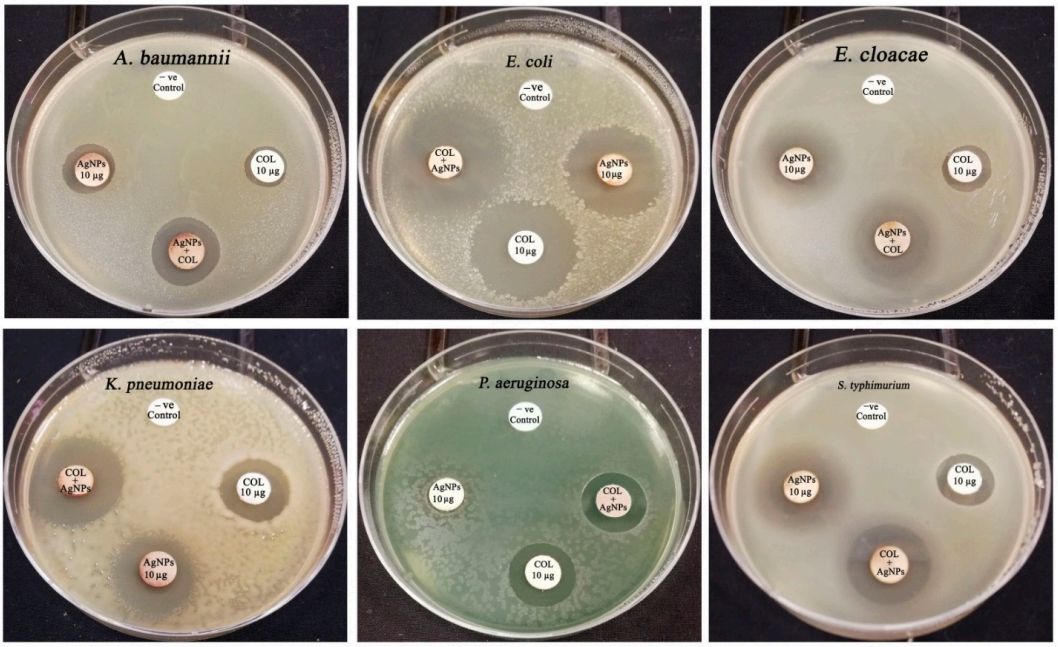

Figure 11. Synergistic antimicrobial efficacy of colistin antibiotic with the biosynthesized AgNPs against the concerned bacterial pathogens.

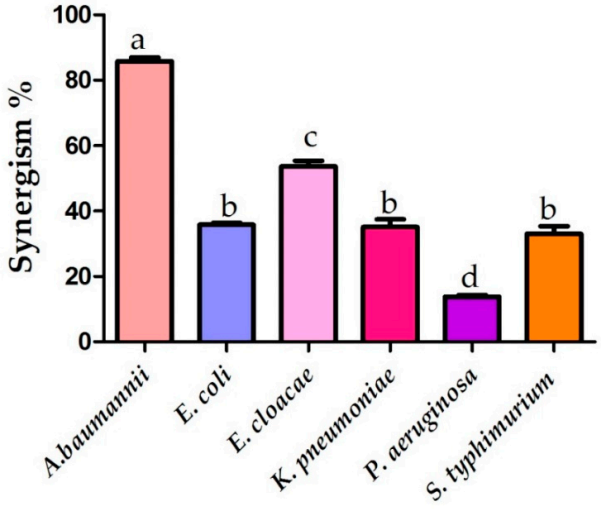

Figure 12. Synergistic percentages of the green synthesized silver nanomaterials with colistin antibiotic (different letters indicate values that were significantly different ($p \leq 0.05$)).

Table 3. Synergistic antibacterial activity of the biogenic AgNPs with colistin antibiotic against the tested strains.

The Tested Strains	Inhibition Zone Diameter (mm)			
	Colistin (10 µg/Disk)	AgNPs (10 µg/Disk)	Colistin (10 µg/Disk) + AgNPs (10 µg/Disk)	Negative Control
A. baumannii	10.12 ± 0.09	14.89 ± 0.53	18.78 ± 0.16	0.00 ± 0.00
E. coli	26.34 ± 0.21	26.34 ± 0.34	35.76 ± 0.48	0.00 ± 0.00
E. cloacae	13.89 ± 0.23	16.89 ± 0.42	21.34 ± 0.35	0.00 ± 0.00
K. pneumoniae	19.89 ± 0.39	20.78 ± 0.13	26.89 ± 0.27	0.00 ± 0.00
P. aeruginosa	15.63 ± 0.14	8.93 ± 0.07	17.78 ± 0.19	0.00 ± 0.00
S. typhimurium	16.45 ± 0.37	18.23 ± 0.29	21.89 ± 0.11	0.00 ± 0.00

Due to their broad range of antiviral, antibacterial, and antimycotic efficiency, silver ions are common antimicrobial agents [94]. Hence, silver ions (Ag^+) are attractive agents for the synthesis of antibacterial materials because of their broad-spectrum antibacterial action [95]. The inactivation of membrane-bound proteins, which alters the shape of cells, inhibits cell division, and disturbs solute and electron transport systems, is the antibacterial mechanism of silver ions [96]. These can prevent the formation of crucial cell constituents such as adenosine triphosphate (ATP) by interfering with DNA and critical enzymes. Multiple locations can be targeted by silver ions, which is useful for preventing the emergence of drug-resistant strains [97].

Collectively, we hypothesized that the synergistic behavior of the colistin and AgNPs combinations could be attributed to both colistin and AgNPs targeting different cellular targets. In this setting, the main target of colistin antibiotic is lipopolysaccharide, which is the core constituent of the outer membrane of Gram-negative bacteria [98]. Furthermore, because colistin antibiotic is a positively charged molecule, it has a great affinity for the negatively charged lipid A molecule of lipopolysaccharide in the outer membrane of bacterial cells, causing cations to be displaced by electrostatic interactions, resulting in membrane disruption and the release of lipopolysaccharide [99]. As a result, colistin disrupts membrane permeability by introduction into the lipophilic acid-fat chain of the outer membrane, resulting in inner membrane disorganization and loss of phospholipid bilayer integrity, culminating in the release of intracellular components and cell death induction [100]. Taken together, the synergistic antibacterial action was thought to be caused by the action of the antibiotic colistin, which damaged the outer membrane of bacterial cells, allowing silver nanoparticles to enter and interact with other cellular components such as DNA, protein, and cell membrane, leading to their disruption by the action of reactive oxygen species [101].

The particle size distribution histogram showed that the particles size falls mostly in the range between 5 and 35 nm, which is a suitable nanosize for different applications. The PDI value was slightly higher than 0.5 (exactly 0.582) and the antimicrobial studies confirmed their potent activity against the tested multidrug-resistant pathogens. Then, the antimicrobial studies were further investigated by detecting the possible synergism between the synthesized nanoparticles and colistin antibiotic. The results affirmed the synergistic activity of the biosynthesized nanomaterials with colistin, confirming the potent bioactivity of the biogenic AgNPs. However, chemical modification of the biosynthesized AgNPs with a stabilizing agent, such as poly(vinyl alcohol) (PVA), could be a suitable solution for the non-homogenous distribution of the biosynthesized AgNPs as it plays an important role in shape-controlled seeded growth and colloidal stability as demonstrated by previous reports [102,103].

4. Conclusions

Salvia officinalis extract mediated green formulation of AgNPs with significant antibacterial effectiveness against different nosocomial and multidrug-resistant bacterial pathogens. The potent antibacterial efficacy could be assigned to the unique physicochemical characteristics of the biogenic AgNPs such as the small particle size diameter of 17.615 $\pm$ 1.24 nm and negative surface charge of -16.2 mV. Furthermore, biogenic AgNPs showed synergistic effectiveness with the antibiotic colistin against the tested strains, displaying the maximum synergism against colistin-resistant *A. baumannii*. As a result, biosynthesized AgNPs could be utilized to formulate highly effective antibacterial agents in combination with the antibiotic colistin to combat nosocomial infections caused by multidrug-resistant bacterial pathogens. In addition, the colistin–AgNPs combination could be utilized to synthesize antimicrobial coatings for use in intensive care units, enabling effective control of nosocomial bacterial infections.

Author Contributions: Conceptualization, M.T.Y. and A.A.A.-A.; methodology, M.T.Y.; software, M.T.Y.; validation, M.T.Y., A.A.A.-A. and F.O.A.-O.; formal analysis, M.T.Y., A.A.A.-A., F.O.A.-O. and A.A.-F.M.; investigation, M.T.Y.; resources, A.A.A.-A.; data curation, M.T.Y.; writing—original draft preparation, M.T.Y.; writing—review and editing, M.T.Y., A.A.-F.M., A.A.A.-A. and F.O.A.-O.; visualization, A.A.-F.M.; supervision, A.A.A.-A. and F.O.A.-O.; project administration, A.A.A.-A.; funding acquisition, A.A.-F.M. All authors have read and agreed to the published version of the manuscript.

Funding: This research project was supported by a grant from the Researchers Supporting Project number (RSP-2021/114), King Saud University, Riyadh, Saudi Arabia.

Institutional Review Board Statement: Not applicable.

Informed Consent Statement: Not applicable.

Data Availability Statement: The datasets used and/or analyzed during the current study are available from the corresponding author upon reasonable request.

Acknowledgments: The authors would like to extend their sincere appreciation to the Researchers Supporting Project number (RSP-2021/114), King Saud University, Riyadh, Saudi Arabia.

Conflicts of Interest: The authors declare no conflict of interest.

References

1. Catalano, A.; Iacopetta, D.; Ceramella, J.; Scumaci, D.; Giuzio, F.; Saturnino, C.; Aquaro, S.; Rosano, C.; Sinicropi, M.S. Multidrug Resistance (MDR): A Widespread Phenomenon in Pharmacological Therapies. *Molecules* **2022**, *27*, 616. [CrossRef] [PubMed]
2. Dadgostar, P. Antimicrobial resistance: Implications and costs. *Infect. Drug Resist.* **2019**, *12*, 3903. [CrossRef] [PubMed]
3. Mancuso, G.; Midiri, A.; Gerace, E.; Biondo, C. Bacterial Antibiotic Resistance: The Most Critical Pathogens. *Pathogens* **2021**, *10*, 1310. [CrossRef] [PubMed]
4. Kyriakidis, I.; Vasileiou, E.; Pana, Z.D.; Tragiannidis, A. *Acinetobacter baumannii* antibiotic resistance mechanisms. *Pathogens* **2021**, *10*, 373. [CrossRef] [PubMed]
5. Nguyen, M.; Joshi, S.G. Carbapenem resistance in *Acinetobacter baumannii*, and their importance in hospital-acquired infections: A scientific review. *J. Appl. Microbiol.* **2021**, *131*, 2715–2738. [CrossRef]
6. Moubareck, C.A. Polymyxins and bacterial membranes: A review of antibacterial activity and mechanisms of resistance. *Membranes* **2020**, *10*, 181. [CrossRef] [PubMed]
7. Eze, E.C.; El Zowalaty, M.E.; Pillay, M. Antibiotic resistance and biofilm formation of *Acinetobacter baumannii* isolated from high-risk effluent water in tertiary hospitals in South Africa. *J. Glob. Antimicrob. Resist.* **2021**, *27*, 82–90. [CrossRef] [PubMed]
8. Lim, S.M.S.; Abidin, A.Z.; Liew, S.M.; Roberts, J.A.; Sime, F.B. The global prevalence of multidrug-resistance among Acinetobacter baumannii causing hospital-acquired and ventilator-associated pneumonia and its associated mortality: A systematic review and meta-analysis. *J. Infect.* **2019**, *79*, 593–600.
9. Navon-Venezia, S.; Kondratyeva, K.; Carattoli, A. *Klebsiella pneumoniae*: A major worldwide source and shuttle for antibiotic resistance. *FEMS Microbiol. Rev.* **2017**, *41*, 252–275. [CrossRef] [PubMed]
10. Choby, J.E.; Howard-Anderson, J.; Weiss, D.S. Hypervirulent *Klebsiella pneumoniae*–clinical and molecular perspectives. *J. Intern. Med.* **2020**, *287*, 283–300. [CrossRef] [PubMed]
11. Poovieng, J.; Sakboonyarat, B.; Nasomsong, W. Bacterial etiology and mortality rate in community-acquired pneumonia, healthcare-associated pneumonia and hospital-acquired pneumonia in Thai university hospital. *Sci. Rep.* **2022**, *12*, 9004. [CrossRef] [PubMed]
12. Martin, R.M.; Bachman, M.A. Colonization, infection, and the accessory genome of *Klebsiella pneumoniae*. *Front. Cell. Infect. Microbiol.* **2018**, *8*, 4. [CrossRef] [PubMed]
13. Zheng, S.H.; Cao, S.J.; Xu, H.; Feng, D.; Wan, L.P.; Wang, G.J.; Xiao, X.G. Risk factors, outcomes and genotypes of carbapenem-non susceptible *Klebsiella pneumoniae* bloodstream infection: A three-year retrospective study in a large tertiary hospital in Northern China. *Infect. Dis.* **2018**, *50*, 443–451. [CrossRef]
14. Annavajhala, M.K.; Gomez-Simmonds, A.; Uhlemann, A.C. Multidrug-resistant Enterobacter cloacae complex emerging as a global, diversifying threat. *Front. Microbiol.* **2019**, *10*, 44. [CrossRef]
15. Aurilio, C.; Sansone, P.; Barbarisi, M.; Pota, V.; Giaccari, L.G.; Coppolino, F.; Barbarisi, A.; Passavanti, M.B.; Pace, M.C. Mechanisms of action of carbapenem resistance. *Antibiotics* **2022**, *11*, 421. [CrossRef] [PubMed]
16. Zaha, D.C.; Bungau, S.; Aleya, S.; Tit, D.M.; Vesa, C.M.; Popa, A.R.; Pantis, C.; Maghiar, O.A.; Bratu, O.G.; Furau, C.; et al. What antibiotics for what pathogens? The sensitivity spectrum of isolated strains in an intensive care unit. *Sci. Total Environ.* **2019**, *687*, 118–127. [CrossRef] [PubMed]
17. Tilahun, M. Emerging Carbapenem-Resistant Enterobacteriaceae Infection, Its Epidemiology and Novel Treatment Options: A Review. *Infect. Drug Resist.* **2021**, *14*, 4363. [CrossRef] [PubMed]

18. Sumbana, J.; Santona, A.; Fiamma, M.; Taviani, E.; Deligios, M.; Chongo, V.; Sacarlal, J.; Rubino, S.; Paglietti, B. Polyclonal emergence of MDR Enterobacter cloacae complex isolates producing multiple extended spectrum beta-lactamases at Maputo Central Hospital, Mozambique. *Rend. Lincei Sci. Fis. Nat.* **2022**, *33*, 39–45. [CrossRef]
19. Guiton, P.S.; Hung, C.S.; Hancock, L.E.; Caparon, M.G.; Hultgren, S.J. Enterococcal biofilm formation and virulence in an optimized murine model of foreign body-associated urinary tract infections. *Infect. Immun.* **2010**, *78*, 4166–4175. [CrossRef] [PubMed]
20. Lee, D.S.; Lee, S.J.; Choe, H.S. Community-acquired urinary tract infection by Escherichia coli in the era of antibiotic resistance. *Biomed Res. Int.* **2018**, *2018*, 7656752. [CrossRef] [PubMed]
21. Farahat, E.M.; Hassuna, N.A.; Hammad, A.M.; Fattah, M.A.; Khairalla, A.S. Distribution of integrons and phylogenetic groups among Escherichia coli causing community-acquired urinary tract infection in Upper Egypt. *Can. J. Microbiol.* **2021**, *67*, 451–463. [CrossRef]
22. Chemaly, R.F.; Simmons, S.; Dale, C., Jr.; Ghantoji, S.S.; Rodriguez, M.; Gubb, J.; Stachowiak, J.; Stibich, M. The role of the healthcare environment in the spread of multidrug-resistant organisms: Update on current best practices for containment. *Ther. Adv. Infect. Dis.* **2014**, *2*, 79–90. [CrossRef] [PubMed]
23. Khan, H.A.; Ahmad, A.; Mehboob, R. Nosocomial infections and their control strategies. *Asian Pac. J. Trop. Biomed.* **2015**, *5*, 509–514. [CrossRef]
24. Velásquez-Garcia, L.; Mejia-Sanjuanelo, A.; Viasus, D.; Carratalà, J. Causative Agents of Ventilator-Associated Pneumonia and Resistance to Antibiotics in COVID-19 Patients: A Systematic Review. *Biomedicines* **2022**, *10*, 1226. [CrossRef] [PubMed]
25. Yassin, M.T.; Mostafa, A.A.F.; Al-Askar, A.A.; Sayed, S.R. In vitro antimicrobial activity of Thymus vulgaris extracts against some nosocomial and food poisoning bacterial strains. *Process Biochem.* **2022**, *115*, 152–159. [CrossRef]
26. Hoffmann, S.; Batz, M.B.; Morris, J.R. Annual cost of illness and quality-adjusted life year losses in the United States due to 14 foodborne pathogens. *J. Food Prot.* **2012**, *75*, 1292–1302. [CrossRef]
27. Arshad, R.; Pal, K.; Sabir, F.; Rahdar, A.; Bilal, M.; Shahnaz, G.; Kyzas, G.Z. A review of the nanomaterials use for the diagnosis and therapy of *Salmonella typhi*. *J. Mol. Struct.* **2021**, *1230*, 129928. [CrossRef]
28. Blair, J.; Webber, M.A.; Baylay, A.J.; Ogbolu, D.O.; Piddock, L.J. Molecular mechanisms of antibiotic resistance. *Nat. Rev. Microbiol.* **2015**, *13*, 42–51. [CrossRef] [PubMed]
29. Wang, L.; Hu, C.; Shao, L. The antimicrobial activity of nanoparticles: Present situation and prospects for the future. *Int. J. Nanomed.* **2017**, *12*, 1227. [CrossRef]
30. Raliya, R.; Singh Chadha, T.; Haddad, K.; Biswas, P. Perspective on nanoparticle technology for biomedical use. *Curr. Pharm. Des.* **2016**, *22*, 2481–2490. [CrossRef] [PubMed]
31. Singh, S.; Arkoti, N.K.; Verma, V.; Pal, K. Nanomaterials and Their Distinguishing Features. In *Nanomaterials for Advanced Technologies*; Springer: Singapore, 2022; pp. 1–18.
32. Hemeg, H.A. Nanomaterials for alternative antibacterial therapy. *Int. J. Nanomed.* **2017**, *12*, 8211. [CrossRef]
33. Slavin, Y.N.; Asnis, J.; Häfeli, U.O.; Bach, H. Metal nanoparticles: Understanding the mechanisms behind antibacterial activity. *J. Nanobiotechnol.* **2017**, *15*, 65. [CrossRef] [PubMed]
34. Mousavi, S.M.; Hashemi, S.A.; Ghasemi, Y.; Atapour, A.; Amani, A.M.; Savar Dashtaki, A.; Babapoor, A.; Arjmand, O. Green synthesis of silver nanoparticles toward bio and medical applications: Review study. *Artif. Cells Nanomed. Biotechnol.* **2018**, *46* (Suppl. 3), S855–S872. [CrossRef]
35. Yassin, M.T.; Mostafa, A.A.F.; Al-Askar, A.A.; Al-Otibi, F.O. Synergistic Antifungal Efficiency of Biogenic Silver Nanoparticles with Itraconazole against Multidrug-Resistant Candidal Strains. *Crystals* **2022**, *12*, 816. [CrossRef]
36. Yaqoob, A.A.; Umar, K.; Ibrahim, M.N.M. Silver nanoparticles: Various methods of synthesis, size affecting factors and their potential applications–a review. *Appl. Nanosci.* **2020**, *10*, 1369–1378. [CrossRef]
37. Shreyash, N.; Bajpai, S.; Khan, M.A.; Vijay, Y.; Tiwary, S.K.; Sonker, M. Green synthesis of nanoparticles and their biomedical applications: A review. *ACS Appl. Nano Mater.* **2021**, *4*, 11428–11457. [CrossRef]
38. Bhardwaj, B.; Singh, P.; Kumar, A.; Kumar, S.; Budhwar, V. Eco-friendly greener synthesis of nanoparticles. *Adv. Pharm. Bull.* **2020**, *10*, 566. [CrossRef] [PubMed]
39. Ramalingam, B.; Parandhaman, T.; Das, S.K. Antibacterial effects of biosynthesized silver nanoparticles on surface ultrastructure and nanomechanical properties of gram-negative bacteria viz. *Escherichia coli* and *Pseudomonas aeruginosa*. *ACS Appl. Mater. Interfaces* **2016**, *8*, 4963–4976. [CrossRef] [PubMed]
40. Ghorbani, A.; Esmaeilizadeh, M. Pharmacological properties of Salvia officinalis and its components. *J. Tradit. Complement. Med.* **2017**, *7*, 433–440. [CrossRef] [PubMed]
41. Balčiūnaitienė, A.; Liaudanskas, M.; Puzerytė, V.; Viškelis, J.; Janulis, V.; Viškelis, P.; Griškonis, E.; Jankauskaitė, V. *Eucalyptus globulus* and *Salvia officinalis* extracts mediated green synthesis of silver nanoparticles and their application as an antioxidant and antimicrobial agent. *Plants* **2022**, *11*, 1085. [CrossRef]
42. Sharifi, F.; Sharififar, F.; Soltanian, S.; Doostmohammadi, M.; Mohamadi, N. Synthesis of silver nanoparticles using Salvia officinalis extract: Structural characterization, cytotoxicity, antileishmanial and antimicrobial activity. *Nanomed. Res. J.* **2020**, *5*, 339–346.
43. Alqasim, A. Colistin-resistant Gram-negative bacteria in Saudi Arabia: A literature review. *J. King Saud Univ. Sci.* **2021**, *33*, 101610. [CrossRef]

44. Longo, L.G.; de Sousa, V.S.; Kraychete, G.B.; Justo-da-Silva, L.H.; Rocha, J.A.; Superti, S.V.; Bonelli, R.R.; Martins, I.S.; Moreira, B.M. Colistin resistance emerges in pandrug-resistant *Klebsiella pneumoniae* epidemic clones in Rio de Janeiro, Brazil. *Int. J. Antimicrob. Agents* **2019**, *54*, 579–586. [CrossRef] [PubMed]
45. Bahador, A.; Taheri, M.; Pourakbari, B.; Hashemizadeh, Z.; Rostami, H.; Mansoori, N.; Raoofian, R. Emergence of rifampicin, tigecycline, and colistin-resistant *Acinetobacter baumannii* in Iran; spreading of MDR strains of novel International Clone variants. *Microb. Drug Resist.* **2013**, *19*, 397–406. [CrossRef] [PubMed]
46. Wi, Y.M.; Choi, J.Y.; Lee, J.Y.; Kang, C.I.; Chung, D.R.; Peck, K.R.; Song, J.H.; Ko, K.S. Emergence of colistin resistance in *Pseudomonas aeruginosa* ST235 clone in South Korea. *Int. J. Antimicrob. Agents* **2017**, *49*, 767–769. [CrossRef]
47. Poirel, L.; Kieffer, N.; Liassine, N.; Thanh, D.; Nordmann, P. Plasmid-mediated carbapenem and colistin resistance in a clinical isolate of *Escherichia coli*. *Lancet Infect. Dis.* **2016**, *16*, 281. [CrossRef]
48. Kim, J.S.; Yu, J.K.; Jeon, S.J.; Park, S.H.; Han, S.; Park, S.H.; Kang, M.; Im Jang, J.; Shin, E.K.; Kim, J.; et al. Distribution of mcr genes among carbapenem-resistant Enterobacterales clinical isolates: High prevalence of mcr-positive Enterobacter cloacae complex in Seoul, Republic of Korea. *Int. J. Antimicrob. Agents* **2021**, *58*, 106418. [CrossRef]
49. Wali, N.; Shabbir, A.; Wajid, N.; Abbas, N.; Naqvi, S.Z.H. Synergistic efficacy of colistin and silver nanoparticles impregnated human amniotic membrane in a burn wound infected rat model. *Sci. Rep.* **2022**, *12*, 6414. [CrossRef]
50. Yassin, M.T.; Mostafa, A.A.F.; Al-Askar, A.A.; Al-Otibi, F.O. Facile Green Synthesis of Zinc Oxide Nanoparticles with Potential Synergistic Activity with Common Antifungal Agents against Multidrug-Resistant Candidal Strains. *Crystals* **2022**, *12*, 774. [CrossRef]
51. Yassin, M.T.; Mostafa, A.A.F.; Al-Askar, A.A.; Alkhelaif, A.S. In vitro antimicrobial potency of *Elettaria cardamomum* ethanolic extract against multidrug resistant of food poisoning bacterial strains. *J. King Saud Univ. Sci.* **2022**, *34*, 102167. [CrossRef]
52. Yassin, M.T.; Mostafa, A.A.; Al-Askar, A.A. Anticandidal and anti-carcinogenic activities of *Mentha longifolia* (Wild Mint) extracts in vitro. *J. King Saud Univ. Sci.* **2020**, *32*, 2046–2052. [CrossRef]
53. Yassin, M.T.; Al-Askar, A.A.; Mostafa, A.A.F.; El-Sheikh, M.A. Bioactivity of *Syzygium aromaticum* (L.) Merr. & LM Perry extracts as potential antimicrobial and anticancer agents. *J. King Saud Univ. Sci.* **2020**, *32*, 3273–3278.
54. Ahmed, F.; AlOmar, S.Y.; Albalawi, F.; Arshi, N.; Dwivedi, S.; Kumar, S.; Shaalan, N.M.; Ahmad, N. Microwave Mediated Fast Synthesis of Silver Nanoparticles and Investigation of Their Antibacterial Activities for Gram-Positive and Gram-Negative Microorganisms. *Crystals* **2021**, *11*, 666. [CrossRef]
55. Yi, Y.; Wang, C.; Cheng, X.; Yi, K.; Huang, W.; Yu, H. Biosynthesis of Silver Nanoparticles by Conyza canadensis and Their Antifungal Activity against Bipolaris maydis. *Crystals* **2021**, *11*, 1443. [CrossRef]
56. Singh, P.; Pandit, S.; Garnæs, J.; Tunjic, S.; Mokkapati, V.R.S.S.; Sultan, A.; Thygesen, A.; Mackevica, A.; Mateiu, R.V.; Daugaard, A.E.; et al. Green synthesis of gold and silver nanoparticles from Cannabis sativa (industrial hemp) and their capacity for biofilm inhibition. *Int. J. Nanomed.* **2018**, *13*, 3571–3591. [CrossRef] [PubMed]
57. Clinical and Laboratory Standards. *Performance Standards for Antimicrobial Disk Susceptibility Tests*; Approved Standard M2-A8; Clinical and Laboratory Standards Institute (CLSI): Wayne, PA, USA, 2003.
58. Yassin, M.T.; Mostafa, A.A.F.; Al Askar, A.A. In Vitro Evaluation of Biological Activities and Phytochemical Analysis of Different Solvent Extracts of *Punica granatum* L. (Pomegranate) Peels. *Plants* **2021**, *10*, 2742. [CrossRef]
59. Punjabi, K.; Mehta, S.; Chavan, R.; Chitalia, V.; Deogharkar, D.; Deshpande, S. Efficiency of biosynthesized silver and zinc nanoparticles against multi-drug resistant pathogens. *Front. Microbiol.* **2018**, *9*, 2207. [CrossRef]
60. Yassin, M.T.; Mostafa, A.A.F.; Al-Askar, A.A. In vitro anticandidal potency of *Syzygium aromaticum* (clove) extracts against vaginal candidiasis. *BMC Complement. Altern. Med.* **2020**, *20*, 25. [CrossRef]
61. Huang, W.; Yan, M.; Duan, H.; Bi, Y.; Cheng, X.; Yu, H. Synergistic antifungal activity of green synthesized silver nanoparticles and epoxiconazole against *Setosphaeria turcica*. *J. Nanomater.* **2020**, *2020*, 9535432. [CrossRef]
62. Lo, W.H.; Deng, F.S.; Chang, C.J.; Lin, C.H. Synergistic antifungal activity of chitosan with fluconazole against *Candida albicans*, *Candida tropicalis*, and fluconazole-resistant strains. *Molecules* **2020**, *25*, 5114. [CrossRef]
63. Moteriya, P.; Padalia, H.; Chanda, S. Characterization, synergistic antibacterial and free radical scavenging efficacy of silver nanoparticles synthesized using *Cassia roxburghii* leaf extract. *J. Genet. Eng. Biotechnol.* **2017**, *15*, 505–513. [CrossRef]
64. Lashin, I.; Fouda, A.; Gobouri, A.A.; Azab, E.; Mohammedsaleh, Z.M.; Makharita, R.R. Antimicrobial and in vitro cytotoxic efficacy of biogenic silver nanoparticles (Ag-NPs) fabricated by callus extract of *Solanum incanum* L. *Biomolecules* **2021**, *11*, 341. [CrossRef]
65. Luna-Sánchez, J.L.; Jiménez-Pérez, J.L.; Carbajal-Valdez, R.; Lopez-Gamboa, G.; Pérez-González, M.; Correa-Pacheco, Z.N. Green synthesis of silver nanoparticles using Jalapeño Chili extract and thermal lens study of acrylic resin nanocomposites. *Thermochim. Acta* **2019**, *678*, 178314. [CrossRef]
66. Hassan, K.T.; Ibraheem, I.J.; Hassan, O.M.; Obaid, A.S.; Ali, H.H.; Salih, T.A.; Kadhim, M.S. Facile green synthesis of Ag/AgCl nanoparticles derived from Chara algae extract and evaluating their antibacterial activity and synergistic effect with antibiotics. *J. Environ. Chem. Eng.* **2021**, *9*, 105359. [CrossRef]
67. Shameli, K.; Ahmad, M.B.; Zargar, M.; Yunus, W.M.Z.W.; Rustaiyan, A.; Ibrahim, N.A. Synthesis of silver nanoparticles in montmorillonite and their antibacterial behavior. *Int. J. Nanomed.* **2011**, *6*, 581. [CrossRef] [PubMed]
68. Tippayawat, P.; Phromviyo, N.; Boueroy, P.; Chompoosor, A. Green synthesis of silver nanoparticles in aloe vera plant extract prepared by a hydrothermal method and their synergistic antibacterial activity. *PeerJ* **2016**, *4*, e2589. [CrossRef]

69. Dhar, S.A.; Chowdhury, R.A.; Das, S.; Nahian, M.K.; Islam, D.; Gafur, M.A. Plant-mediated green synthesis and characterization of silver nanoparticles using *Phyllanthus emblica* fruit extract. *Mater. Today Proc.* **2021**, *42*, 1867–1871. [CrossRef]
70. Khalifa, K.S.; Hamouda, R.A.; Hanafy, D.; Hamza, A. In vitro antitumor activity of silver nanoparticles biosynthesized by marine algae. *Dig. J. Nanomater. Biostruct.* **2016**, *11*, 213–221.
71. Jakinala, P.; Lingampally, N.; Hameeda, B.; Sayyed, R.Z.; Khan, M.Y.; Elsayed, E.A.; El Enshasy, H. Silver nanoparticles from insect wing extract: Biosynthesis and evaluation for antioxidant and antimicrobial potential. *PLoS ONE* **2021**, *16*, e0241729.
72. Ahmad, A.; Wei, Y.; Syed, F.; Tahir, K.; Rehman, A.U.; Khan, A.; Ullah, S.; Yuan, Q. The effects of bacteria-nanoparticles interface on the antibacterial activity of green synthesized silver nanoparticles. *Microb. Pathog.* **2017**, *102*, 133–142. [CrossRef]
73. Ghaedi, M.; Yousefinejad, M.; Safarpoor, M.; Khafri, H.Z.; Purkait, M.K. Rosmarinus officinalis leaf extract mediated green synthesis of silver nanoparticles and investigation of its antimicrobial properties. *J. Ind. Eng. Chem.* **2015**, *31*, 167–172. [CrossRef]
74. Ravichandran, S.; Paluri, V.; Kumar, G.; Loganathan, K.; Kokati Venkata, B.R. A novel approach for the biosynthesis of silver oxide nanoparticles using aqueous leaf extract of Callistemon lanceolatus (Myrtaceae) and their therapeutic potential. *J. Exp. Nanosci.* **2016**, *11*, 445–458. [CrossRef]
75. Islam, S.N.; Naqvi, S.M.A.; Parveen, S.; Ahmad, A. Application of mycogenic silver/silver oxide nanoparticles in electrochemical glucose sensing; alongside their catalytic and antimicrobial activity. *3 Biotech* **2021**, *11*, 342. [CrossRef] [PubMed]
76. Mistry, H.; Thakor, R.; Patil, C.; Trivedi, J.; Bariya, H. Biogenically proficient synthesis and characterization of silver nanoparticles employing marine procured fungi *Aspergillus brunneoviolaceus* along with their antibacterial and antioxidative potency. *Biotechnol. Lett.* **2021**, *43*, 307–316. [CrossRef]
77. AbdelRahim, K.; Mahmoud, S.Y.; Ali, A.M.; Almaary, K.S.; Mustafa, A.E.Z.M.; Husseiny, S.M. Extracellular biosynthesis of silver nanoparticles using *Rhizopus stolonifer*. *Saudi J. Biol. Sci.* **2017**, *24*, 208–216. [CrossRef] [PubMed]
78. Habeeb Rahuman, H.B.; Dhandapani, R.; Narayanan, S.; Palanivel, V.; Paramasivam, R.; Subbarayalu, R.; Thangavelu, S.; Muthupandian, S. Medicinal plants mediated the green synthesis of silver nanoparticles and their biomedical applications. *IET Nanobiotechnol.* **2022**, *16*, 115–144. [CrossRef]
79. Alahmad, A.; Feldhoff, A.; Bigall, N.C.; Rusch, P.; Scheper, T.; Walter, J.G. *Hypericum perforatum* L.-mediated green synthesis of silver nanoparticles exhibiting antioxidant and anticancer activities. *Nanomaterials* **2021**, *11*, 487. [PubMed]
80. Aabed, K.; Mohammed, A.E. Synergistic and Antagonistic Effects of Biogenic Silver Nanoparticles in Combination with Antibiotics Against Some Pathogenic Microbes. *Front. Bioeng. Biotechnol.* **2021**, *9*, 249. [CrossRef]
81. Badawy, A.M.E.; Luxton, T.P.; Silva, R.G.; Scheckel, K.G.; Suidan, M.T.; Tolaymat, T.M. Impact of environmental conditions (pH, ionic strength, and electrolyte type) on the surface charge and aggregation of silver nanoparticles suspensions. *Environ. Sci. Technol.* **2010**, *44*, 1260–1266. [CrossRef]
82. Sun, B.; Liu, H.; Jiang, Y.; Shao, L.; Yang, S.; Chen, D. New mutations involved in colistin resistance in *Acinetobacter baumannii*. *Msphere* **2020**, *5*, e00895-19. [CrossRef]
83. Olaitan, A.O.; Morand, S.; Rolain, J.M. Mechanisms of polymyxin resistance: Acquired and intrinsic resistance in bacteria. *Front. Microbiol.* **2014**, *5*, 643. [CrossRef] [PubMed]
84. Qamer, S.; Romli, M.H.; Che-Hamzah, F.; Misni, N.; Joseph, N.M.; Al-Haj, N.A.; Amin-Nordin, S. Systematic Review on Biosynthesis of Silver Nanoparticles and Antibacterial Activities: Application and Theoretical Perspectives. *Molecules* **2021**, *26*, 5057. [CrossRef]
85. Makvandi, P.; Wang, C.Y.; Zare, E.N.; Borzacchiello, A.; Niu, L.N.; Tay, F.R. Metal-based nanomaterials in biomedical applications: Antimicrobial activity and cytotoxicity aspects. *Adv. Funct. Mater.* **2020**, *30*, 1910021. [CrossRef]
86. Gold, K.; Slay, B.; Knackstedt, M.; Gaharwar, A.K. Antimicrobial activity of metal and metal-oxide based nanoparticles. *Adv. Ther.* **2018**, *1*, 1700033. [CrossRef]
87. Pal, A.; Bhattacharjee, S.; Saha, J.; Sarkar, M.; Mandal, P. Bacterial survival strategies and responses under heavy metal stress: A comprehensive overview. *Crit. Rev. Microbiol.* **2022**, *48*, 327–355. [CrossRef] [PubMed]
88. Gunawan, C.; Faiz, M.B.; Mann, R.; Ting, S.R.; Sotiriou, G.A.; Marquis, C.P.; Amal, R. Nanosilver targets the bacterial cell envelope: The link with generation of reactive oxygen radicals. *ACS Appl. Mater. Interfaces* **2020**, *12*, 5557–5568. [CrossRef]
89. Durán, N.; Durán, M.; De Jesus, M.B.; Seabra, A.B.; Fávaro, W.J.; Nakazato, G. Silver nanoparticles: A new view on mechanistic aspects on antimicrobial activity. *Nanomed. Nanotechnol. Biol. Med.* **2016**, *12*, 789–799. [CrossRef]
90. Yassin, M.T.; Mostafa, A.A.F.; Al-Askar, A.A.; Al-Otibi, F.O. Facile green synthesis of silver nanoparticles using aqueous leaf extract of *Origanum majorana* with potential bioactivity against multidrug resistant bacterial strains. *Crystals* **2022**, *12*, 603. [CrossRef]
91. Lopez-Carrizales, M.; Velasco, K.I.; Castillo, C.; Flores, A.; Magaña, M.; Martinez-Castanon, G.A.; Martinez-Gutierrez, F. In vitro synergism of silver nanoparticles with antibiotics as an alternative treatment in multiresistant uropathogens. *Antibiotics* **2018**, *7*, 50. [CrossRef]
92. Deng, H.; McShan, D.; Zhang, Y.; Sinha, S.S.; Arslan, Z.; Ray, P.C.; Yu, H. Mechanistic study of the synergistic antibacterial activity of combined silver nanoparticles and common antibiotics. *Environ. Sci. Technol.* **2016**, *50*, 8840–8848. [CrossRef] [PubMed]
93. Panáček, A.; Smékalová, M.; Kilianová, M.; Prucek, R.; Bogdanová, K.; Večeřová, R.; Kolář, M.; Havrdová, M.; Płaza, G.A.; Chojniak, J.; et al. Strong and nonspecific synergistic antibacterial efficiency of antibiotics combined with silver nanoparticles at very low concentrations showing no cytotoxic effect. *Molecules* **2015**, *21*, 26. [CrossRef] [PubMed]

94. Wahid, F.; Zhong, C.; Wang, H.S.; Hu, X.H.; Chu, L.Q. Recent advances in antimicrobial hydrogels containing metal ions and metals/metal oxide nanoparticles. *Polymers* **2017**, *9*, 636. [CrossRef]
95. Zhao, X.Q.; Wahid, F.; Zhao, X.J.; Wang, F.P.; Wang, T.F.; Xie, Y.Y.; Jia, S.-R.; Zhong, C. Fabrication of amino acid-based supramolecular hydrogel with silver ions for improved antibacterial properties. *Mater. Lett.* **2021**, *300*, 130161. [CrossRef]
96. Khattak, S.; Qin, X.T.; Wahid, F.; Huang, L.H.; Xie, Y.Y.; Jia, S.R.; Zhong, C. Permeation of silver sulfadiazine into TEMPO-oxidized bacterial cellulose as an antibacterial agent. *Front. Bioeng. Biotechnol.* **2021**, *8*, 616467. [CrossRef] [PubMed]
97. Wahid, F.; Zhao, X.J.; Jia, S.R.; Bai, H.; Zhong, C. Nanocomposite hydrogels as multifunctional systems for biomedical applications: Current state and perspectives. *Compos. B Eng.* **2020**, *200*, 108208. [CrossRef]
98. Da Silva, G.J.; Domingues, S. Interplay between colistin resistance, virulence and fitness in *Acinetobacter baumannii*. *Antibiotics* **2017**, *6*, 28. [CrossRef] [PubMed]
99. Ledger, E.V.; Sabnis, A.; Edwards, A.M. Polymyxin and lipopeptide antibiotics: Membrane-targeting drugs of last resort. *Microbiology* **2022**, *168*, 001136. [CrossRef]
100. Yi, K.; Liu, S.; Liu, P.; Luo, X.; Zhao, J.; Yan, F.; Pan, Y.; Liu, J.; Zhai, Y.; Hu, G. Synergistic antibacterial activity of tetrandrine combined with colistin against MCR-mediated colistin-resistant Salmonella. *Biomed. Pharmacother.* **2022**, *149*, 112873. [CrossRef]
101. Ribeiro, A.I.; Dias, A.M.; Zille, A. Synergistic effects between metal nanoparticles and commercial antimicrobial agents: A Review. *ACS Appl. Nano Mater.* **2022**, *5*, 3030–3064. [CrossRef]
102. Kyrychenko, A.; Pasko, D.A.; Kalugin, O.N. Poly (vinyl alcohol) as a water protecting agent for silver nanoparticles: The role of polymer size and structure. *Phys. Chem. Chem. Phys.* **2017**, *19*, 8742–8756. [CrossRef]
103. Mandal, P.; Ghosh, S. Green Approach to the Synthesis of Poly (Vinyl Alcohol)-Silver Nanoparticles Hybrid Using Rice Husk Extract and Study of its Antibacterial Activity. *Biointerface Res. Appl. Chem.* **2020**, *10*, 6474–6480.